Discrete Chemical Release From a Microfluidic Chip

Min Hu, *Member, IEEE*, Timo Lindemann, Thorsten Göttsche, Joerg Kohnle,
Roland Zengerle, *Member, IEEE*, and Peter Koltay

Abstract—We demonstrate a discrete chemical release method, capable of delivering picoliter volumes of chemical solutions with 100 μm of spatial resolution and 20 μs of response time. The releasing mechanism is based on the transfer of pulsed liquid plugs through a hydrophobic air chamber. A microfluidic chip consisting of such a releasing array (2×10) is designed and fabricated. Numerical simulation and experimental testing are performed to verify the working principle. Advantages of this release-on-demand technology include leakage-free, fast response and versatile control of release profile. This new method could be a key enabling technology for precisely controlled release of biochemicals for modern pharmacological and biological research. **[2006-0253]**

Index Terms—Air gap, discrete chemical stimulation, microfluidic chip, picoliter chemical release, pulsed liquid ejection.

I. INTRODUCTION

CONTROLLED release refers to the process in which an appropriate amount of drugs or biochemical agents is released to the target as a function of time, site, or stimuli. The purpose of controlled release is to achieve a highly optimized efficacy of drug therapy or biochemical stimulation, or to reduce drug administrations and increase patient compliance [1]. For instance, one object of pharmaceutical controlled release is to deliver drugs to the proper site in order to trigger and maintain the therapeutic action for a prolonged period of time. In biological study, controlled release can be used to locally deliver a certain amount of biochemicals (at predefined release profile) to cells to observe their response.

The technique by which a biochemical compound is released can have significant effect on the therapeutic or biological efficacy [2]. To release drugs/biochemicals in a predesigned manner, many techniques have been reported for different applications, ranging from core-shell nanoparticles for stimuli-sensitive cancer therapy [3] to micromachined piezoelectric

pump for precise insulin infusion [4]. Most of these techniques fall into two categories: *in vivo* matrix-based systems and *ex vivo* microdevice-based systems. While the matrix-based systems can be biodegradable, which means no surgery is required to implant or remove the systems [5], [6]; microdevice-based systems can provide greater temporal and spatial control over the drug release process [7]. For example, a solid-state silicon microchip presented by Santini *et al.* [8] can release single or multiple chemical compounds in small volumes at multiple well-defined locations. This microchip releases chemicals by electrochemical dissolution of thin anode membranes, which seal the micro drug-loaded compartments on the chip. Another example is a self-regulated drug delivery device, based on the integration of both mechanical and chemical methods [9]. Using a pH-sensitive hydrogel switch to regulate the drug release, a constant release rate can be obtained from this device by carefully designing the shape of the drug reservoir. In addition, microfabricated needle arrays have also been demonstrated for painless and prolonged transdermal drug release [10], [11].

The combination of microsystems and biotechnology in recent years is not only extending the techniques for controlled drug delivery but also expanding the application areas for controlled release. For example, a microfluidic chip has been presented for use in a prototype retinal interface [12]–[14]. This chip is capable of repetitively releasing neurotransmitter in small volumes at multiple locations. Another example for controlled release in biotechnology is the localized chemical stimulation of micropatterned cells for bioassays [15]. Cell-based bioassay can be used for cytotoxic evaluation, drug screening, and environmental monitoring. For the study of intracellular communication, implantable polyimide microprobes have been demonstrated, which allow simultaneous, selective chemical delivery/probing and multichannel recording/stimulation of bioelectric activity [16]. Similar silicon probes with multiple release channels have also been demonstrated for delivering very little amounts of bioactive compounds into highly localized areas of neural tissue while simultaneously recording electrical signals from neurons [17].

In our previous work [18], localized functional chemical stimulation of adherent TE 671 cells was demonstrated by release of calcein AM and acetylcholine through a modular setup of bubble-jet print head. In this paper, we present an integrated approach for precisely controlled delivery of biochemical agents like neurotransmitters to specified regions within a cell culture. Unlike conventional controlled release techniques that deliver chemical agents in a continuous way, our method releases a given dose of biochemical solution in a discrete, repeatable and fast manner. This release-on-demand
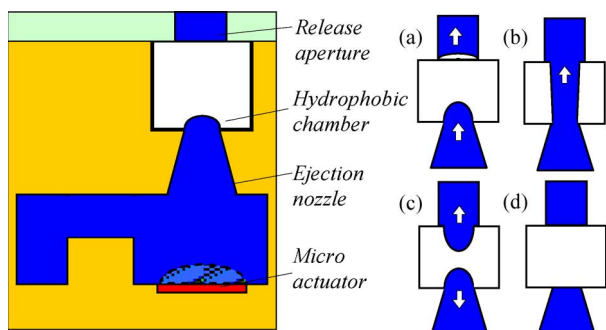
Fig. 1. Working principle of discrete chemical release based on air-gap technology. A hydrophobic air chamber is combined with a burst liquid jet generator and acts as a reversible burst valve. (a)–(d) show that the hydrophobic air chamber normally cuts off the liquid pathway, but allows an ejected liquid plug to pass through it. With sufficient kinetic energy to overcome the surface tension, the ejected liquid plug can fly over the air gap and enter into the opposite release aperture.

technique outperforms those of existing approaches, particularly in volumetric resolution, spatial resolution and control of release profile. The following sections focus on the working principle of the method, its theoretical models and implementation in a microfluidic chip.

II. PRINCIPLE AND THEORETICAL MODELS

A. Working Principle

The main technological challenges for temporally and spatially controlled chemical release are the following: 1) how to swiftly switch ON and OFF a tiny array of release apertures and 2) how to effectively block any possible leakage from the apertures when the drugs or chemicals are not demanded. The latter is a particularly critical issue for functional chemical stimulation in many cellular studies.

To avoid continuous chemical stimulation as a consequence of leakage, our approach uses burst liquid ejection through an air gap for chemical release in chip design (Fig. 1). The release unit considered for this purpose consists of a burst liquid jet generator, a hydrophobic air chamber, and a release aperture. The burst liquid jet generator is used to produce discrete liquid plugs or droplets from the ejecting nozzle with high speed and on demand. Depending on the specific applications, the burst liquid jet generator could be a thermal bubble actuator, or a micropiezoelectric/electrostatic actuator known from different types of inkjet print heads. Because of its simplicity in implementation, however, in this paper we only consider thermal bubble actuation for pulsed liquid plug/droplet generation.

The leakage-blocking hydrophobic air chamber—the key element of the release unit—works as a reversible burst valve. It normally prevents liquid passing through, thus eliminating any possible leakage from the open release aperture. The impingement of ejected liquid plugs in the release aperture will not cause splash of smaller droplets due to larger surface energy required. This means that the pulsed liquid jet will completely enter into the release aperture. As the air in the chamber is not escaping during the liquid ejection, the blocking effect of the hydrophobic chamber can be sustained after each ejection.
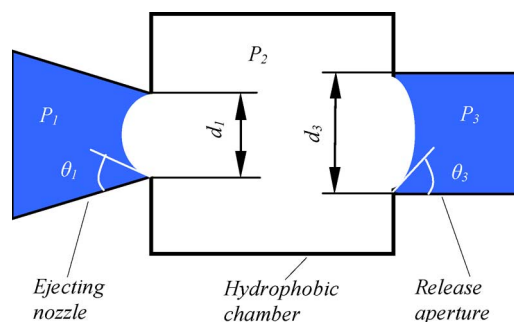

Fig. 2. Liquid holding mechanism by a hydrophobic air chamber. The air gap between the ejecting nozzle and the release aperture severs the flow path. The hydrophobic surface of and the pressure inside the chamber prevent liquid passing through it when no pulsed liquid jet is generated by the micro (thermal bubble) actuator.

Besides preventing leakage, our method also gives an intrinsic advantage over those approaches that are based on diluting the same amount of chemicals in a larger volume. If the chemicals are diluted and delivered in larger liquid volumes to cells, the whole liquid environment of certain cells is replaced by the diluted solution. Our technique allows the delivery of chemical solution in volumes as small as picoliters. In this way, we can swiftly add extremely small amounts of chemicals to cells without displacing the existing liquid environment around a specific cell area.

B. Liquid Holding Mechanism

To illustrate how liquid can be held from leaking by the hydrophobic chamber, Fig. 2 shows a schematic model of the hydrophobic air chamber. Due to the hydrophobic property of the chamber, liquid from the nozzles (by self-priming capillary forces) will not wet the chamber surface. Instead, meniscuses will be formed at the nozzle (or aperture) orifices on both sides of the chamber.

Considering that the force balance on the liquid in the ejection nozzle and according to the Young–Laplace equation [19], we have

$$P_1 - P_2 = \frac{4\sigma \cdot \cos(\pi - \theta_1)}{d_1} \qquad (1)$$

where P_1 is the liquid pressure in the ejection nozzle, P_2 is the air pressure in the hydrophobic chamber, σ is the surface tension of the liquid, d_1 is diameter of the ejection orifice, and θ_1 is the static (equilibrium) contact angle of the liquid at the hydrophobic ejection nozzle, which is defined as the angle on the liquid side of the tangential line drawn through the three-phase boundary where a liquid, gas, and solid intersect.

The pressure that a hydrophobic chamber can withstand is limited. Given a surface material and a liquid, the maximum contact angle is fixed and known as the dynamic advancing contact angle (θ_a). Therefore, the maximum pressure $(P_{1\max})$ that the hydrophobic chamber can resist from the side of ejection nozzle is

$$P_{1\max} = \text{Max}(P_1) = \frac{4\sigma \cdot \cos(\pi - \theta_a)}{d_1} + P_2. \qquad (2)$$

Similarly, considering the force balance on the liquid in the release aperture, we have

$$P_3 - P_2 = \frac{4\sigma \cdot \cos(\pi - \theta_3)}{d_3} \qquad (3)$$

where P_3 is the liquid pressure in the release aperture, d_3 is diameter of the release nozzle, and θ_3 is the static (equilibrium) contact angle of the liquid at the hydrophobic edge of the release aperture. Also, the maximum pressure ($P_{3\,\max}$) that the hydrophobic chamber can resist from the side of the release nozzle is

$$P_{3\,\max} = \mathrm{Max}(P_3) = \frac{4\sigma \cdot \cos(\pi - \theta_a)}{d_3} + P_2. \qquad (4)$$

As long as the liquid pressure on each side of the hydrophobic chamber is lower than the corresponding critical pressure, chemical solution can be held in the ejection nozzle without release or leakage through the air gap. For example, suppose the air pressure in the hydrophobic chamber is the same as atmospheric pressure ($P_2 = P_{\mathrm{atm}}$) and the hydrophobic chamber is completely nonwettable ($\theta_a = 180°$). For a 30-μm ejection nozzle filled with pure water ($\sigma = 7.28 \times 10^{-2}$ N/m), according to (2), the air gap is not leaking up to 103.75 kPa (equivalent gauge pressure 2.43 kPa). Moreover, this critical pressure is also adjustable by regulating the pressure in the hydrophobic chamber (P_2).

C. Dynamics of Liquid Transportation

The transportation of pulsed liquid plug through the air gap can be divided into several steps. First, a liquid jet is formed at the outlet of the ejecting nozzle by the rapid increase of pressure in the nozzle chamber. Then, the ejected liquid jet flies through the air gap. After that, the liquid jet impinges on the liquid surface in the release nozzle and merges into it. Depending on the size of the air gap, the breakup of liquid jet by the decrease of pressure in the ejecting nozzle will occur either before (large air gap) or after (small air gap) the head of liquid plug has merged into the release nozzle.

Suppose the fluid is incompressible and with constant viscosity, the motion of liquid can be described by the Navier–Stokes equation and the mass continuity equation [20]

$$\rho \left(\frac{\partial \vec{v}}{\partial t} + (\vec{v} \cdot \nabla)\vec{v} \right) + \nabla p - \eta \nabla^2 \vec{v} = 0$$

$$\nabla \cdot \vec{v} = 0 \qquad (5)$$

where ρ is the density, $\vec{v} = (u, v, w)$ is the velocity vector, t is a time variable, p is the pressure, η is the dynamic viscosity of the liquid.

The boundary conditions applicable to the control volume are as follows. At the wall of the heater chamber, nozzle, and the release aperture, a no-slip boundary condition is given by

$$\vec{v} = 0. \qquad (6)$$

At the liquid inlet of the heater chamber and the outlet of the release nozzle, constant pressure boundary conditions are, respectively, imposed as

$$p = P_{\mathrm{res}} \qquad (7)$$

and

$$p = P_{\mathrm{ape}} \qquad (8)$$

where P_{res} is the pressure in the liquid reservoir, and P_{ape} is the pressure at the outlet of the release aperture. At the outlet of the ejection nozzle, the inlet of the release aperture and the surface of the liquid jet, a free surface boundary condition can be applied as

$$p = P_2 + \sigma \left(\frac{1}{r_1} + \frac{1}{r_2} \right) \qquad (9)$$

where P_2 is the pressure in the hydrophobic air chamber, r_1 and r_2 are principal radii of the curvature at given point on liquid surface. At the vapor bubble surface, a similar boundary condition is given by

$$p = p_{\mathrm{vap}} + \sigma \left(\frac{1}{r_1} + \frac{1}{r_2} \right) \qquad (10)$$

where p_{vap} is the pressure in the vapor bubble, r_1 and r_2 are principal radii of the curvature at given point on the bubble inner surface.

According to the thermal bubble model developed by Asai [21], the vapor pressure in the thermal bubble can be modeled by an impulsive function

$$p_{\mathrm{vap}} = (P_i - P_s) \exp\left[-\left(\frac{t}{t_0} \right)^{0.5} \right] + P_s \qquad (11)$$

where P_i is the initial bubble pressure that can be determined by using the Clapeyron–Clausius equation [22], P_s is the bubble pressure in the later stage depending on the ambient temperature of the bubble, t_0 is a time constant indicating the speed of pressure decrease which depends on the geometry and the thermal properties of the materials and the profile of heating pulse.

The transportation of the pulsed liquid plug by thermal bubble actuation is a very complicated free surface flow problem [23]–[26]. It depends not only on liquid properties like the viscosity and surface tension but also on the geometry of the ejecting nozzle and liquid velocity distribution in it. The dynamics of this pulsed ejection is complicated also by the fact that, it is an unsteady flow that is a function of time and space in both the ejecting and release nozzles. The highly nonlinear nature of the Navier–Stokes equations that govern fluid flow here prevents explicit analyses of the phenomenon. To evaluate and determine the required pulsed pressure and boundary conditions (including geometries) for liquid plug transportation, in the next section we use computational fluid dynamic (CFD) methods to solve the above system governing equations.
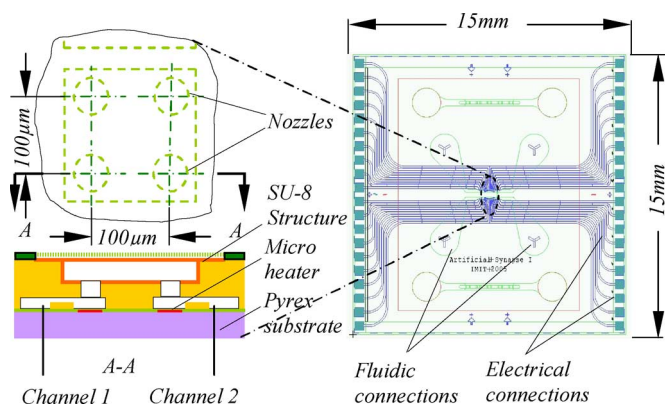
Fig. 3. Design of microchip with integrated air gaps. 20 individually controllable delivery units are evenly deployed on the top center of the chip, forming a 10×2 release array with pitches (spatial resolution) of $100 \times 100\ \mu$m. Each delivery unit has a short structured microfluidic channel, which connects the microheater chamber to the main chemical supply (channel 1 or 2). On top of the microheater chamber is the ejecting nozzle. It is 30 μm in diameter and 35 μm in height. Four ejecting nozzles share a common hydrophobic air chamber on top.
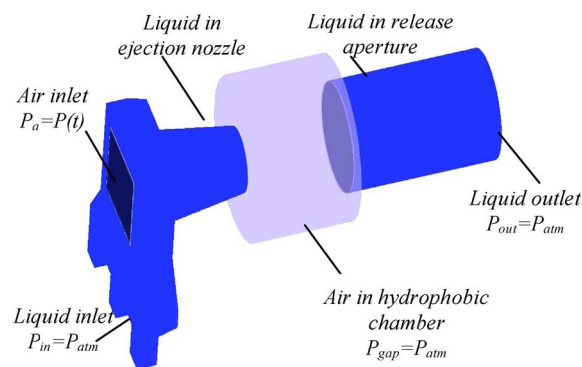

Fig. 4. Schematic 3-D geometric model and boundary conditions of a release unit for CFD simulation. To simplify the simulation: 1) a cylindrical nozzle instead of nanoporous membrane is modeled as release aperture; 2) an individual cylindrical air chamber rather than a shared one is used to neglect the influence from three neighboring nonactive release units and; 3) the thermal bubble actuation is modeled as an air inlet boundary condition at the microheater area in this mode.

III. DESIGN AND SIMULATION

A. Design

Based on the working principle described above, a microfluidic chip is designed for fluid delivery into an aqueous medium via an integrated air-gap chamber. In the design, thermal bubble actuation is chosen for the generation of pulsed liquid plug/droplet.

As shown in Fig. 3, the microchip comprises two main fluidic channels (1 and 2) with 20 individually addressable delivery units connecting to them. These delivery units form a 10×2 delivery array with nozzle diameter of 30 μm and pitch size of 100 μm on the center of the chip. Depending on the application, the microchip surface can be covered with either a layer containing a micromachined release aperture, a nanoporous membrane or a cell culture insert (as in the experiments presented later on) with a porous membrane at the bottom to form the release apertures.

B. Simulation

For discrete chemical release, a complete liquid release cycle includes the energizing of the microheater, bubble nucleation, growth and collapse of vapor bubble, liquid jet formation, breakup and emerging of liquid into release aperture, as well as refilling of the ejecting nozzle. Due to the complexity of the process, it is very difficult to evaluate this dynamic process by theoretically solving the coupled governing equations. To verify the working principle and check the feasibility of the presented chip design, a CFD simulation has been performed which visualizes the dynamic process of a pulsed liquid plug crossing the air gap under thermal bubble actuation. We choose commercially available software, CFD-ACE+ from ESI-CFD, for this simulation work. CFD-ACE+ uses numerical methods to solve both the Navier–Stokes equations and mass continuity equations. It adopts the volume-of-fluid method to model free boundary surfaces. Therefore, this software can simulate 3-D

and complex fluid flows like a liquid plug flying through an air gap.

Fig. 4 shows the 3-D geometric model and the boundary conditions for one release unit of the microfluidic chip. The geometry of the delivery unit is further meshed by 3-D structured grid with cubic cells. The boundary conditions for this simulation are as follows. First, the inner walls of the liquid supply channels, heating chamber, ejection nozzle, and the release aperture are assumed to be full-wetting, whereas the walls of the hydrophobic air chamber are assumed to be nonwetting. Second, the liquid inlet of the model is set at the entrance of the liquid supply channels, whereas the liquid out is set at the exit of the release nozzle. The pressures at the liquid inlet and outlet are considered as atmospheric pressure. Third, the thermal bubble actuation at the microheater area is modeled as an air inlet boundary condition as proposed by Asai, with a time-variable pressure profile described in (11). The bubble growth and collapse is thus approximated by an appropriate airflow through the heater area. Water and air are used as fluids for the simulation. We assume that the water has a density (ρ) of 1000 kg/m^3, a surface tension (σ) of 0.073 N/m, and a dynamic viscosity (η) of 0.00098 kg/m $\cdot$ s, whereas air has a density (ρ) of 1.207 kg/m^3, and a dynamic viscosity (η) of 0.0000182 kg/m $\cdot$ s.

With this setup, a complete release cycle of liquid plug ejection under a pulsed thermal bubble pressure was simulated. The simulation results (Fig. 5) show that corresponding to the bubble growth, a liquid plug can be generated from the ejecting nozzle. Due to the fast dynamics behavior of the bubble actuation, the speed of ejected liquid plug can be very high (about 10 m/s). The liquid plug subsequently flies over the hydrophobic chamber and joins the liquid meniscus in the release nozzle and forms a liquid bridge. Then, the collapse of the thermal bubble cuts off the ejected liquid column. After that the tail of the liquid plug retracts into the release nozzle. Within a single ejection, a liquid amount of 20 pL could be transferred while the nozzle could be refilled for the next ejection in 20 μs of time.
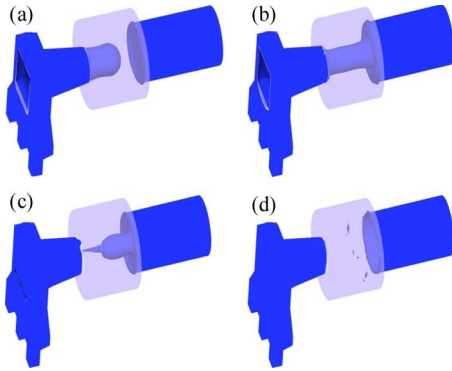
Fig. 5. Simulated process of an ejected liquid plug flying over the hydrophobic air chamber. (a) Liquid jet forming at $t = 2$ μs. (b) Liquid jet bridging the air gap at $t = 4$ μs. (c) Liquid plug breakup at $t = 14$ μs. (d) End of transport process at $t = 28$ μs. Corresponding to the process are the growth and collapse of the "thermal bubble" at the microheater area.
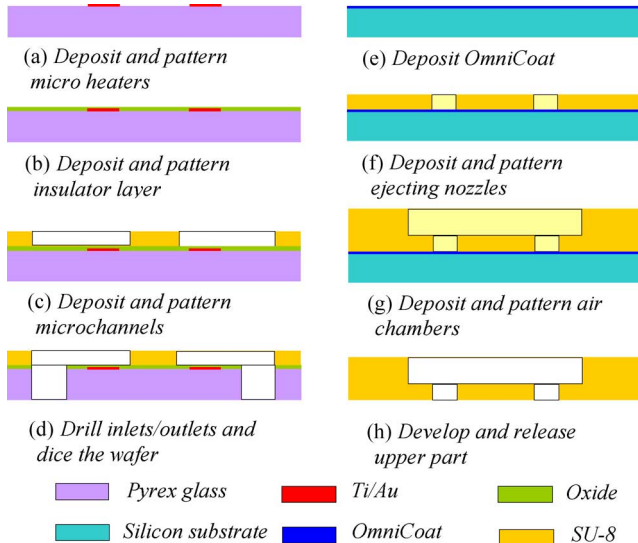

Fig. 6. Schematic diagram of microfabrication procedure for the designed microchip. (a)–(d) Lower part fabrication process. (e)–(h) Upper part fabrication process. Microheaters, electronic interconnections, and open fluidic channels are fabricated on a Pyrex substrate to form the chip lower part. The ejection nozzles and common air chambers which form the chip upper part are made of SU-8.

IV. FABRICATION AND ASSEMBLY

A. Fabrication Process

We chose SU-8 to fabricate the microfluidic structures because of its excellent resistance to chemical treatments and good biocompatibility. As SU-8 is a negative tone resist, however, we could not directly obtain the embedded channels, nozzles and air chambers by sequentially spin-coating and patterning SU-8 layers. We had to use bonding technologies to realize these embedded microstructures. Correspondingly, the fabrication process (Fig. 6) consists of three main steps: 1) fabrication of chip lower part with microheaters, electronic interconnections and open fluidic channels on the Pyrex substrate; 2) preparation of chip upper part with ejection nozzles and hydrophobic air chambers; and 3) bonding of the two parts with adhesive epoxy.
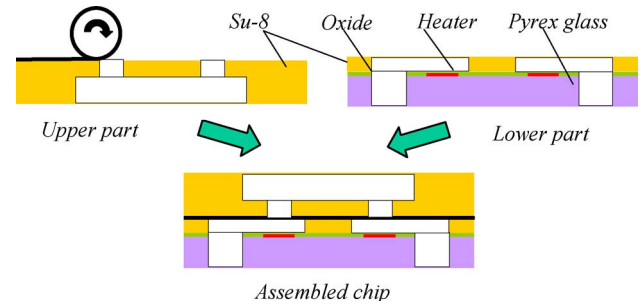

Fig. 7. Adhesive bonding of the two parts by making use of a microassembly system. First, the bonding surfaces of both parts are treated with oxygen plasma. Then, a very thin layer (about 5 μm thick) of adhesive epoxy (EPO-TEK 353ND from Epoxy Technology, Inc.) is evenly applied to the bonding surface of the upper SU-8 structure by a roller. After that, the two parts are held, aligned, and pressed, together with a chip-bonding system (Fineplacer Lambda from Finetech GmbH).

For the fabrication of the lower part of the chip, first a 100-nm-thick titanium layer and a 500-nm-thick gold layer, respectively, were magnetically sputtered and wet etched to form the microheaters and electrical interconnections on the Pyrex substrate. Then, a 2-μm-thick LTO was deposited and patterned on the microheaters and interconnection lines as an insulation layer. After that, a 20-μm-thick SU-8 2025 layer was spin-coated and patterned with open microfluidic channels. Finally, the wafer was diced to chips after the mechanical drilling of the fluidic inlets and outlets on the Pyrex substrate.

The chip's upper part was initially fabricated on a silicon wafer by spin coating and patterning of multilayers of SU-8. First, a very thin layer of OmniCoat was applied to the wafer surface by spin coating for the later release of the SU-8 structures as described in [27]. Then, a 25-μm-thick layer of SU-8 2025 and a 300-μm-thick layer of SU-8 2100 were sequentially spin-coated and lithographically patterned to form the ejection nozzles and air chambers. After that, the wafer was put into SU-8 developer in an ultrasonic bath. Due to the internal stresses of the baked layers the patterned SU-8 structures could be easily released from the silicon substrate.

B. Assembly

Fig. 7 shows the adhesive bonding procedure of the two separately fabricated parts. After bonding, the chip was put into an oven and dried at 80 °C for 30 min. Here, control of the thickness of epoxy is critical for the success of this bonding process. Due to the capillary action of microchannels, the adhesive epoxy could have flown into and totally blocked the microfluidic channels during the bonding or drying process, if the applied epoxy would not have been thin enough.

The hydrophobic coating of the air chambers was performed in the last step. Perfluorodecyldimethylchlorosilane was dropped to the air chambers and then blown away while the microfluidic channels and nozzles were filled with photo resist for protection. Fig. 8 shows an assembled microfluidic chip, together with a microscopic image of the lower part [Fig. 8(a)] and an SEM image of the upper part [Fig. 8(b)] before it was glued and wire-bonded to a printed circuit board for testing.
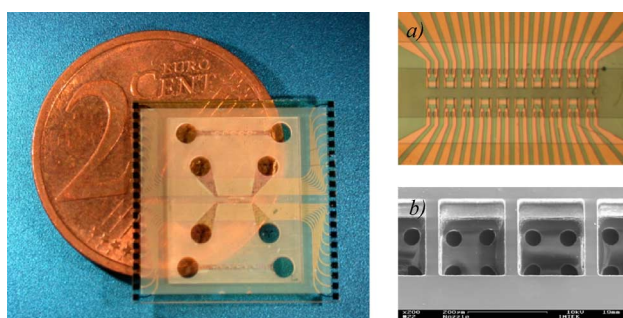
Fig. 8. Assembled microfluidic chip. (a) Microscopic image of the lower part showing the microheaters and open fluidic channels. (b) SEM image of the upper part showing four nozzles within each common air chamber.
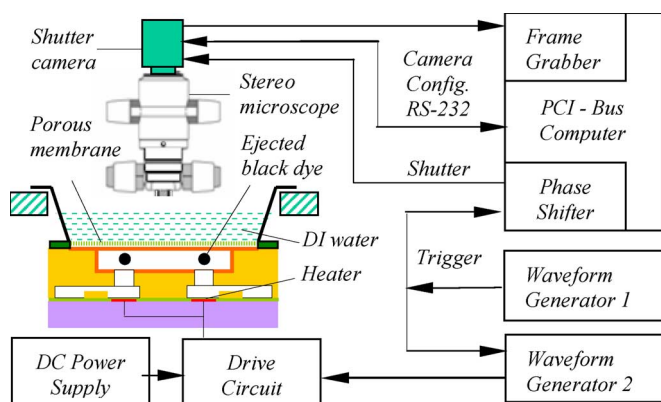

Fig. 9. Experimental setup for the microfluidic chip (drawing not to scale). A cell culture insert with nanoporous membrane is bonded on top of the chip to observe the droplet release. Two arbitrary waveform generators (Agilent 33120A) are connected in burst mode to trigger the microheaters through a driver circuit for power amplification. The triggering signal from the first waveform generator is also used as synchronizing input for the stroboscopic camera to take the image at predefined delay time.

V. EXPERIMENTAL VERIFICATION

A. Experimental Setup

To facilitate the testing, we directly attached a cell culture insert (PICMORG50 from Millipore) with double-sided tape on the top of the microchip to be able to observe droplet transfer (Fig. 9). The insert has a porous membrane bottom with pore size of 0.4 μm. After filling the microfluidic chip with black dye and the insert with DI water, we put the assembly of the microchip under a stereo stroboscopic camera. Two Agilent arbitrary waveform generators (33120A) were connected in burst mode to trigger the microheaters. In this way, both the energizing (heating) time and the working frequency of the heater (therefore the working frequenc of the release unit) under test could be precisely controlled. At the same time, the triggering signal was also used as synchronizing input for the stroboscopic camera. In the following tests, short electric pulses with current amplitude of 0.4 A and pulse width of 2 μs were applied to the microresistive heaters.

B. Results

For the first test, we triggered the microresistive heater under test at a frequency of 5 kHz to observe the burst release of different amounts of black dye within a very short period of time. The results (Fig. 10) show that the delivery unit could continuously work at extremely high speeds. The ejected droplets can fly through the air gap, penetrate the porous membrane and accumulate on the top surface under the water. The amount of black dye is increasing while the number of triggers to the microheater increases. As the volume of a pulsed liquid plug is in picoliter range and its release process only takes submilliseconds, time-varying, and nonlinear drug (or chemical) delivery profiles can be easily realized by this new technology.

From the pictures of Fig. 10, we also find some smaller dark points around the main droplet. The satellite drops cause these as a subsequence of acoustic wave reflection in the ejection nozzle. The existence of satellite drops will affect on the volume accuracy. However, this phenomenon can be prevented by adjusting the static pressure inside the chip (therefore, the position of liquid meniscus in the ejection nozzle). It can also be prevented through a different design—using thermal bubble itself to break up the liquid jet—as described in [28] and [29].

For the second test, the time-resolved concentration of black dye around a delivery aperture was measured to evaluate the generation of chemical microgradients in a cell culture insert. We conducted the experiment by releasing only one drop of black dye to the porous membrane. Then, every second a picture was taken by stroboscopic camera and from the gray scale values of the images the concentration of black dye in the DI water was deduced. As shown in Fig. 11, the black dye diffused within the DI water and the concentration decayed over time. Compared to the droplet release speed, the decay rate of black dye concentration in the DI water is quite slow. This was expected in our setup due to the fact that the released black dye forms a droplet hanging at the bottom of the porous membrane. That droplet continuously delivers dye by diffusion through the porous membrane to the top (water) side.

VI. DISCUSSION

Due to its fast dynamic and on demand characteristics (similar to inkjet printing), this chemical release method has many advantages, which include but are not limited to the following. 1) Accurate delivery—The delivered chemical volume can be precisely controlled; the resolution can be in the picoliter range. 2) Versatile controllability—Zero-oder, time-varying, nonlinear, and even arbitrary delivery profiles can be easily implemented with this rapid and discrete approach. 3) Fast response—The release of chemical could be initiated and stopped within microseconds because of the localized actuation. 4) Repeatable release—Chemical doses can be repeatedly delivered on demand. 5) Leakage free performance—The delivery aperture is completely cutoff by liquid surface tension when the chemical is not demanded. As long as the static pressure in the fluid channel does not exceed the threshold value, no leakage will occur. 6) Efficient delivery—The release of drugs is very effective, no liquid suck back, no extra drug and buffer are lost like in a negative pressure system. 7) Easy integration—The simple design is very suitable for system integration (e.g., for *in vivo* applications), as the pulse pressure generators can be microfabricated with established techniques.
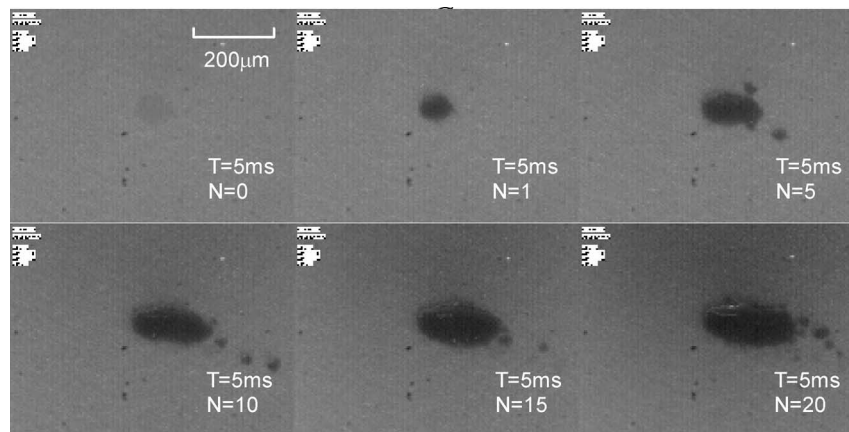
Fig. 10.   Top view of the porous membrane after different numbers of black dye droplets are delivered to the bottom of it. T is the delay time for the stroboscopic image recording that was counted from the first triggering pulse; N stands for the number of trigger signals sent to the microheater (at 5 kHz).
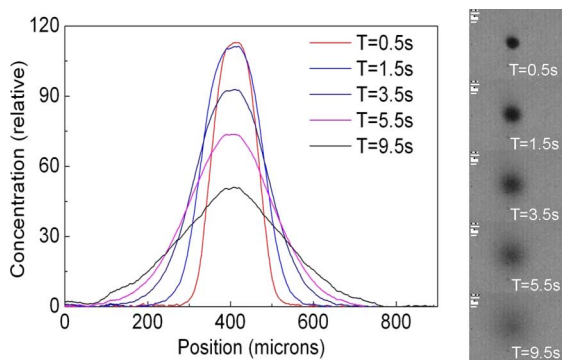

Fig. 11.   Time-resolved concentrations (inverted gray level) of black dye (left) around a release aperture (right) after one drop of dye is released from the microchip. The center of the release aperture is located at a position of $400\ \mu$m from the left side of the observed area. The inverted gray scale values are obtained by a horizontal line cut through the center of the release aperture for each image.

8) Multiple applications—Based on the same working principle, new microfluidic devices and platforms capable of precise volume/concentration control can be built for biomedical diagnostics and analytical chemistry.

VII. CONCLUSION

A novel microfluidic method for temporal and localized chemical release has been demonstrated in this paper. Using hydrophobic air chamber as a reversible burst valve and combining it with a burst liquid jet generator, this method can discretely release picoliter volume of chemicals on demand. Significances of this technology include versatile controllability, leakage free operation, high resolution, and fast response. A microfluidic chip based on this new technology is designed, fabricated and tested by making use of thermal bubble actuation. Spatial resolution of 100 μm, minimum release volume of 20 pL, and maximum release frequency of 5 kHz are achieved in black dye release. This leakage blocking by air gap technique is not limited to the thermal bubble actuation. It is also applicable to piezoelectric or electrostatic actuation for a wide range of temperature-sensitive biochemical release. Future work will be dedicated to the various applications of the presented technology, such as for controlled delivery of drugs and neurotransmitters to the muscle cells and neurons in pharmacological research and for generation of chemical microgradients in cell cultures and tissue regrowth.

REFERENCES

[1] S. Razzacki, P. Thwar, M. Yang, V. Ugaz, and M. Burns, "Integrated microsystems for controlled drug delivery," *Adv. Drug Deliv. Rev.*, vol. 56, no. 2, pp. 185–198, 2004.
[2] A. Grayson, I. Choi, B. Tyler, P. Wang, H. Brem, M. Cima, and R. Langer, "Multi-pulse drug delivery from a resorbable polymeric microchip device," *Nat. Mater.*, vol. 2, no. 11, pp. 767–772, Nov. 2003.
[3] K. Soppimath, C. Tan, and Y. Yang, "pH-Triggered thermally responsive polymer core-shell nanoparticles for targeted drug delivery," *Adv. Mater.*, vol. 17, no. 3, pp. 318–323, Feb. 2005.
[4] D. Maillefer, H. van Lintel, G. Rey-mermet, and R. Hirschi, "A high-performance silicon micropump for an implantable drug delivery system," in *Proc. IEEE MEMS*, 1999, vol. 12, pp. 541–546.
[5] L. Brannon-Peppas, "Polymers in controlled drug delivery," *Med. Plast. Biomater.*, vol. 4, no. 6, pp. 34–44, 1997.
[6] J. West, "Drug delivery: Pulsed polymers," *Nat. Mater*, vol. 2, no. 11, pp. 709–710, Nov. 2003.
[7] A. Grayson, R. Shawgo, Y. Li, and M. Cima, "Electronic MEMS for triggered delivery," *Adv. Drug Deliv. Rev.*, vol. 56, no. 2, pp. 173–184, 2004.
[8] J. Santini, Jr., M. Cima, and R. Langer, "A controlled-release microchip," *Nature*, vol. 397, no. 6717, pp. 335–338, Jan. 1999.
[9] X. Cao, S. Lai, and J. Lee, "Design of a self-regulated drug delivery device," *Biomed. Microdevices*, vol. 3, no. 2, pp. 109–118, Jun. 2001.
[10] D. McAllister *et al.*, "Microfabricated needles for transdermal delivery of macromolecules and nanoparticles: Fabrication methods and transport studies," *Proc. Nat. Acad. Sci.*, vol. 100, no. 24, pp. 13755–13760, Nov. 2003.
[11] P. Griss and G. Stemme, "Side-opened out-of-plane microneedles for microfluidic transdermal liquid transfer," *J. Microelectromech. Sys.*, vol. 12, no. 3, pp. 296–301, Jun. 2003.
[12] M. Peterman, J. Nooland, M. Blumenkranz, and H. Fishman, "Localized chemical release from an artificial synapse chip," *Proc. Nat. Acad. Sci.*, vol. 101, no. 27, pp. 9951–9954, Jul. 2004.

[13] M. Peterman *et al.*, "Localized neurotransmitter release for use in a prototype retinal interface," *Invest. Ophthalmol. Vis. Sci.*, vol. 44, no. 7, pp. 3144–3149, Jul. 2003.

[14] J. Noolandi, M. C. Peterman, P. Huie, C. Lee, M. S. Blumenkranz, and H. A. Fishman, "Towards a neurotransmitter-based retinal prosthesis using an inkjet print-head," *Biomed. Microdevices*, vol. 5, no. 3, pp. 195–199, Sep. 2003.

[15] H. Kaji, M. Nishizawa, and T. Matsue, "Localized chemical stimulation to micropatterned cells using multiple laminar fluid flows," *Lab Chip*, vol. 3, no. 3, pp. 208–211, Aug. 2003.

[16] S. Metz, A. Bertsch, D. Bertrand, and P. Renaud, "Flexible polyimide probes with microelectrodes and embedded microfluidic channels for simultaneous drug delivery and multi-channel monitoring of bioelectric activity," *Biosens. Bioelectron.*, vol. 19, no. 10, pp. 1309–1318, May 2004.

[17] J. Chen, K. Wise, J. Hetke, and S. Bledsoe, Jr., "A multichannel neural probe for selective chemical delivery at the cellular level," *IEEE Trans. Biomed. Eng.*, vol. 44, no. 8, pp. 760–769, Aug. 1997.

[18] S. Zibek, P. Koltay, M. Hu, R. Zengerle, W. Nisch, A. Stett, and M. Stelzle, "Localized functional chemical stimulation of TE 671 cells adherent on nanoporous membrane by calcein and acetylcholine," *Biophys. J.-Biophys. Lett.*, to be published.

[19] D.-S. Meng, T. Cubaud, C.-M. Ho, and C.-J. C. Kim, "A membrane breather for micro fuel cell with high concentration methanol," in *Proc. Hilton Head: A Solid State Sensor, Actuator and Microsyst. Workshop*, Hilton Head Island, SC, 2004, pp. 141–144.

[20] A. Asai, "Three-dimensional calculation of bubble growth and drop ejection in a bubble jet," *Trans. ASME, J. Fluids Eng.*, vol. 114, no. 4, pp. 638–641, 1992.

[21] A. Asai, "Bubble dynamics in boiling under high heat flux pulse heating," *Trans. ASME, J. Heat Transfer*, vol. 113, no. 4, pp. 973–979, 1991.

[22] G. Castellan, *Physical Chemistry*, 3rd ed, vol. 89. London, U.K.: Addison-Wesley, 1983.

[23] J. Dijksman, "Hydrodynamics of small tubular pumps," *J. Fluid Mech.*, vol. 139, pp. 173–191, 1984.

[24] R. Badie and D. Lange, "Mechanism of drop constriction in a drop-on-demand inkjet system," *Proc. R. Soc. Lond. A, Math. Phys. Sci.*, vol. 453, no. 1967, pp. 2573–2581, Dec. 1997.

[25] J. Fromm, "Numerical calculation of the fluid dynamics of drop-on-demand jets," *IBM J. Res. Develop.*, vol. 28, no. 3, pp. 322–333, May 1984.

[26] S. Middleman, *Modeling Axisymmetric Flows—Dynamics of Films, Jets, and Drops*. London, U.K.: Academic, 1995.

[27] B. Bohl, R. Steger, R. Zengerle, and P. Koltay, "Multi-layer SU-8 lift-off technology for microfluidic devices," *J. Micromech. Microeng.*, vol. 15, no. 6, pp. 1125–1130, Jun. 2005.

[28] F. Tseng, C. Kim, and C. Ho, "A high-resolution high-frequency monolithic top-shooting microinjector free of satellite drops—Part I: Concept, design, and model," *J. Microelectromech. Syst.*, vol. 11, no. 5, pp. 427–436, Oct. 2002.

[29] F. Tseng, C. Kim, and C. Ho, "A high-resolution high-frequency monolithic top-shooting microinjector free of satellite drops—Part II: Fabrication, implementation, and characterization," *J. Microelectromech. Syst.*, vol. 11, no. 5, pp. 437–447, Oct. 2002.

Timo Lindemann received the Diploma degree in microsystem technology from the Department of Microsystems Engineering (IMTEK), University of Freiburg, Freiburg, Germany, in 2002. His thesis involved research on the temperature distribution in microhotplates.

From August 2002 to February 2006, he was a Ph.D. student at the IMTEK—Laboratory for Microelectromechanical Systems Applications, where he worked within the "IDEAL" project developing a new kind of 1-in thermal bubble jet printhead and dealing with the 3-D computational fluid dynamic simulations of free jet dosage systems. In February 2006, he joined Robert Bosch GmbH, Stuttgart Sindelfingen, Germany.

Thorsten Göttsche received the Diploma degree in mechanical engineering, focusing on the subject piezoelectrically controlled microvalves, from the University of Stuttgart, Stuttgart, Germany, in 2001.

In 1999, he worked for six months at Nihon Kohden Corporation, Tokyo, Japan, in the Microsensor Department. Since 2001, he has been a member of the Microfluidics Department at the Institute for Micromachining and Information Technology of the Hahn-Schickard-Gesellschaft, Villingen-Schwenningen, Germany. His main scientific focus is on assembly technology and microfluidics, particularly drug delivery systems.

Min Hu (M'99) received the Ph.D. degree in precision instruments from Tsinghua University, Beijing, China, in 1997.

From 1997 to 2001, he was with Nanyang Technological University, Singapore, working on research and development of miniature electromechanical systems. From 2001 and 2002, he was a Research Scientist with the University of Central Florida. Currently, he is a Senior Scientist in the Department of Microsystems Engineering, University of Freiburg, Freiburg, Germany. His research and development interests include microactuators and sensors, microfluidic devices and systems, microfabrication, miniature linear/spherical motors, precision motion control, and intelligent mechatronic systems.

Joerg Kohnle received the degree in physical engineering from the University of Applied Sciences (UAS) of Zwickau.

He has a proven track record as Project Manager in the Microfluidics Group of the Institute for Micromachining and Information Technology of the Hahn-Schickard-Gesellschaft, Villingen-Schwenningen, Germany, working on various projects involving precision dosage systems, making him an expert in the field of microfluidics with more than six years experience in the field.

Roland Zengerle (M'05) studied physics at the Technical University of Munich, Munich, Germany, where he received the Ph.D. degree with the development of an electrostatistically driven micropump.

He is currently the Head of the Laboratory for Microelectromechanical Systems (MEMS) Applications in the Department of Microsystems Engineering, University of Freiburg, Freiburg, Germany. In addition, he is also a Director at the Institute for Micromachining and Information Technology of the Hahn-Schickard-Gesellschaft, Villingen-Schwenningen, Germany. His research is focused on microfluidics and covers topics like miniaturized and autonomous dosage systems, nanoliter and picoliter dispensing, lab-on-a-chip systems, miniaturized fuel cells, as well as micro- and nanofluidics simulation. He has coauthored more than 200 technical publications and 25 patents. He is the European Editor of the *Springer Journal of Microfluidics and Nanofluidics*.

Dr. Zengerle serves on the international steering committee of the IEEE MEMS Conference, as well as on the technical program committee of the biannual actuator conference.

Peter Koltay received the Ph.D. degree in physics from the Albert Ludwigs University, Freiburg, Germany, in 1999.

From 1999 to 2005, he was a Group Leader and Assistant Lecturer in the Department of Microsystems Engineering (IMTEK), University of Freiburg. In 2005, he founded the company BioFluidix GmbH, which he has been leading since then as Managing Director. In 2006, he was appointed as Chief Engineer and Deputy of Prof. Zengerle at IMTEK, and since then, he has been working with both BioFluidix and IMTEK to combine his professional and scientific interests. His scientific interests include the physics of droplet generation, microdispensing devices like ink-jet printers, as well as their applications. He is also interested in modeling and simulation of microfluidic systems, in particular, computational fluid dynamic simulations of free surfaces with focus on applications to direct methanol microfuel cells (μDMFC) and droplet generation systems.